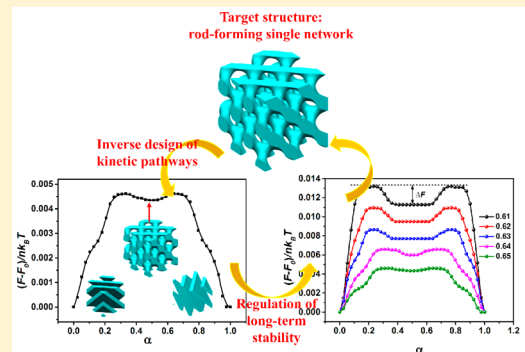


## Construction of Rod-Forming Single Network Mesophases in Rod-Coil Diblock Copolymers via Inversely Designed Phase Transition Pathways

Tongjie Sun, Faqiang Liu, Ping Tang,\*<sup>†</sup> Feng Qiu, and Yuliang Yang

State Key Laboratory of Molecular Engineering of Polymers, Department of Macromolecular Science, Fudan University, Shanghai 200433, China

**ABSTRACT:** The string method is introduced to the self-consistent mean-field theory for rod-coil diblock copolymers to investigate the phase transition kinetics. The equal arc length parametrization used in our improved string method is constrained on both the density and orientation order parameters to obtain accurate and stable minimum energy pathways (MEP). Focusing on different single networks formed by rods as the target structures, we developed an inverse design strategy of kinetic pathways. By designing distinct initial structures (lamellae or cylinders) with specific symmetry matching the target structure as the two ends of the string, we calculated the MEP and analyzed the effects of chain rigidity on the phase transition kinetics. The results indicate that the reordering transition between lamellae belonging to the same crystallographic plane group can induce the formation of metastable single networks. The shape and arrangement of the rigid rods will influence the epitaxial phase transition. The long-term stability of the target structures can be regulated by tailoring the block composition as well as the geometrical asymmetry between rigid and flexible segments, which may guide the experiments to fabricate long-lived single networks.



### I. INTRODUCTION

Nonequilibrium self-assembled structures are widely observed in block copolymers and provide exciting opportunities for polymer engineering practice.<sup>1–3</sup> The emergence of intricate nonequilibrium structures is controlled by dynamic processes. Because of the multiscale characteristics, block copolymers are usually trapped in some metastable structures occurring in the order-order transition (OOT) pathways. For example, perforated lamellae (PL) are frequently observed in experiments as intermediate structures before the formation of double gyroid (DG).<sup>4–8</sup> In addition, various external fields can induce complicated phase transitions, resulting in a variety of nonequilibrium structures. For example, large-amplitude oscillatory shearing can induce phase transition from O<sup>70</sup> to O<sup>52</sup>.<sup>9</sup> Recent experiments by Kim et al.<sup>10</sup> show that different thermal processing conditions (annealing modes) can induce distinct complex metastable structures, such as C14 and C15 quasi-crystalline structures. The phase structures with similar structural elements are in close proximity to each other in the free energy landscape. The disturbance of experimental conditions can easily induce their transitions. For example, the OOTs between gyroid (G), diamond (D), and plumber's nightmare (P) mesophases with similar triply periodic minimal surfaces (TPMS) have been confirmed experimentally.<sup>11–15</sup>

With advances in synthesis methods and characterization techniques, an increasing number of block copolymers with sophisticated molecular characteristics have been synthesized. This generates a wider parameter space as well as more

complex self-assembled structures.<sup>1,16–18</sup> Correspondingly, more competitive metastable structures emerge. Therefore, dynamic process control plays an increasingly significant role in practical applications. However, there are relatively few theoretical studies related to phase transition kinetics. For flexible block copolymer systems, the OOT kinetics investigation has made some progress, mainly focusing on the phase transition epitaxy, nucleation information, and metastable states in kinetic paths. On the basis of the self-consistent mean-field theory (SCFT) calculations and detailed exploration of Landau's free energy landscape, Matsen constructed OOT paths between different ordered phases, including cylinder-DG<sup>19</sup> and cylinder-sphere transformations.<sup>20</sup> He confirmed that the phase transitions proceed through the nucleation and growth mechanism. Using classical nucleation theory, Wickham et al.<sup>21</sup> studied the nucleation process of stable cylinders from metastable lamellae and obtained the size of the nonspherical critical nuclei via the Wulff construction. Wang and Jiang<sup>22</sup> found that the epitaxial relationship originates from the matching of the dominant Fourier components of the structures. In recent years, the combination of the string method and other theoretical simulation methods (such as the SCFT) has become a robust tool for studying phase transition kinetics.<sup>23–28</sup> Exploiting this tool, Cheng et

Received: April 11, 2018

Revised: June 10, 2018

Published: July 24, 2018

al.<sup>23</sup> not only obtained detailed information on the critical nucleus in various phase transitions but also predicted that the lamellae-to-DG transition follows a two-step nucleation mechanism through the PL. Using the same method, our previous research found that the epitaxial growth between lamellae and DG with similar unit cell size is prone to occur.<sup>24</sup>

Nevertheless, for the block copolymers with chain rigidity, the numerical treatment is very difficult because of the anisotropic orientation interaction between the rigid components as well as the conformational asymmetry effect between the rigid and flexible components.<sup>29–35</sup> High orientation interaction will drive the rigid or semiflexible segments to align in parallel along a particular direction, giving rise to the self-assembled structures exhibiting liquid crystal behavior. This liquid crystal effect tends to drive the block copolymers to self-assemble into interesting lamellar structures.<sup>36–38</sup> For example, rigid blocks can be arranged in a single- or double-layer mode; their orientation can be along the normal direction of the layer (smectic A) or with a certain angle to it (smectic C).<sup>29,39–42</sup> This liquid crystal effect together with the geometrical asymmetry effect will have great influence on the phase transition kinetics, and there is no relevant theoretical reports on them. In experiments, there has been preliminary progress.<sup>43–45</sup> In the solution system, the block copolymers with chain rigidity are found to form an ellipsoidal structure, and the introduction of gold nanoparticles induces the transition from ellipsoids to hollow vesicles.<sup>46</sup> The phase transitions between liquid crystal structures with rigid blocks forming the matrix in rod-coil diblock copolymers have been observed,<sup>47</sup> which is inconsistent with the theoretically calculated asymmetric phase diagrams.<sup>30,32</sup> The new experimental phenomena require theoretical investigations to further explore the mechanisms and thus guide practice. Therefore, this article focuses on the theoretical investigation about the OOT kinetics of rod-coil diblock copolymers.

Although the molecular topology design stabilizes many metastable structures,<sup>16,48</sup> the single network mesophases are still metastable. Because metastable structures play an increasingly critical role in experiments,<sup>10</sup> the fabrication of single networks with long-term stability via dynamic process control becomes a promising route. For experimental researchers, rod-coil block copolymers have the natural advantages of preparing single networks. First, rod-coil block polymers can withstand more severe experimental conditions for the preparation of single networks and contribute to the reduction of defect densities. In experiments, double networks or alternating networks are usually used as templates to obtain single networks by means of etching, calcination, and so forth.<sup>49–52</sup> These routes are creative and effective yet may be easy to damage the networks and cause defects. In rod-coil block copolymers, there are obvious chemical differences between rigid and flexible segments; for example, rigid blocks usually contain aromatic or conjugated groups.<sup>53–55</sup> Thus, when we try to remove the matrix and get the single networks, higher temperatures or more solvents can be selected, bringing great convenience to the experimental preparation. Second, because of the good mechanical properties as well as optical and electrical properties of the rod components, the resulting rigid networks, namely the networks formed by rods, resemble nanoparticle-filling networks.<sup>56,57</sup> Therefore, it is of more practical significance to study the formation kinetics of single networks in rod-coil block copolymers.

Progress in the experimental synthesis methods has created a huge parameter space, which brings convenience to experimenters; on the other hand, it is difficult to navigate through this huge design space and quickly screen suitable molecular structures for a target structure.<sup>1</sup> Fortunately, the inverse design strategies developed in recent years establish better connections between theory and experiment.<sup>58,59</sup> On the basis of this idea, we expect to develop an inverse design strategy of kinetic pathways in rod-coil blocks. The traditional research method starts from a specific phase transition path and determines the metastable structures that are encountered in this pathway.<sup>23,24,60–62</sup> The inverse approach, however, takes an opposite route: starting from the target structure and searching for the phase transition pathways on which the same one occurs. On the basis of this idea, we first construct the initial states that have a matching relationship with the target single networks; then, we inversely engineer the kinetic pathways. Finally, we try to regulate the long-term stability of the target single networks in the obtained pathways to make them easier to be observed in experiments. This inverse design strategy does not aim at the design of new molecular topologies but focuses on simple rod-coil block copolymers and searches for the kinetic pathways to the target structures from the existing easy-to-prepare simple phases such as lamellae and cylinders. In the process of inverse kinetic pathway design, the key is to determine the symmetry (crystallographic plane or direction) of the initial and terminal structures in the pathways.

In this study, we introduce the string method into the SCFT of rod-coil diblock copolymers to develop a theoretical method for studying the phase transition kinetics of block copolymers with chain rigidity. Because of the orientation of the rigid segments and the orientation interactions between them, research on the self-assembly behavior of the chain rigidity-containing system presents a huge challenge in terms of numerical solutions and computational efficiency.<sup>29–34</sup> In this case, when the string method is introduced to analyze the phase transition kinetics of self-assembled structures due to the emergence of a variety of intermediate states (including various transient and metastable structures) with complex curvatures in the kinetic pathways, numerical solutions become more difficult. Therefore, the development of efficient and stable numerical methods is key to studying the phase transition mechanism of rod-coil block copolymers. To ensure the calculation stability and obtain an effective minimum energy pathway (MEP), we improve the string method for the flexible block copolymers, i.e., enforce the equal arc length restriction on the orientation order parameters. Meanwhile, we choose the simple phases (lamellae, cylinders) that are very close to each other in the free energy landscape as the two ends of the string and carry out the calculations within a single unit cell. Thus, we need to precisely design the structures at both ends of the string to ensure a good match between them. The initialized string is generated using linear interpolation, which can be used to scan the metastable states in the phase transition pathways. We have also adopted a multithreaded calculation method to further improve computational efficiency. Using the above method, we calculated the phase transition kinetics of rod-coil block copolymers, and analyzed the effect of the configurational asymmetry between rigid and flexible components and the liquid crystal behavior on the phase transitions. Using the inverse strategy of kinetic pathways, we successfully constructed different single networks

via designed kinetic pathways and realized the fabrication of long-lived metastable single networks.

## II. THEORY AND NUMERICAL METHODS

**Self-Consistent Mean-Field Theory (SCFT).** The SCFT used to predict the self-assembly behavior of rod-coil diblock copolymers is the same as our recent work,<sup>63</sup> and its detailed derivation was first described by Pryamitsyn and Ganesan.<sup>29</sup> Here, we give a brief introduction. Consider an incompressible system containing  $n$  rod-coil block copolymer chains with a volume of  $V$ . Each chain contains  $N_R$  rigid segments and  $N_C$  flexible segments with  $N = N_C + N_R$  denoting the total chain length. Assuming that the rigid and flexible segments possess the same bulk number density  $\rho_0 = nN/V$ , then the volume fractions for coil and rod blocks are  $f_C = N_C/N$  and  $f_R = N_R/N = 1 - f_C$ , respectively. The flexible blocks are described using a Gaussian chain model ( $0 \leq s \leq f_C$ ), and the rigid blocks are described using a rigid rod model ( $f_C < s \leq 1$ ). The statistical segment lengths for rod and coil blocks are  $b = l_R/N_R$  ( $l_R$ : the rod block length) and  $a$  (Kuhn length), respectively. Another parameter,  $\beta = bN/a\sqrt{(N/6)}$ , is thus introduced to characterize the conformational asymmetry effect between the rod and coil blocks.  $\beta$  indicates the shape of the rod (length-to-diameter ratio). Small  $\beta$  corresponds to stubby rods, whereas large  $\beta$  corresponds to slim rods.

The free energy functional of a single chain of the system, which can be divided into physically relevant contributions, interfacial energy  $F_{\text{inter}}$ , entropic energy  $-TS$ , and orientation interaction energy  $F_{\text{orien}}$ , satisfies the equation

$$\frac{F}{nk_B T} = \frac{1}{V} \int d\mathbf{r} \left\{ \chi N \phi_R(\mathbf{r}) \phi_C(\mathbf{r}) - \sum_{P=R,C} \omega_P(\mathbf{r}) \phi_P(\mathbf{r}) \right. \\ \left. + \eta(\mathbf{r}) \left( \sum_{P=R,C} \phi_P(\mathbf{r}) - 1 \right) - \frac{\mu N}{2} \mathbf{S}(\mathbf{r}) : \mathbf{S}(\mathbf{r}) + \mathbf{M}(\mathbf{r}) : \mathbf{S}(\mathbf{r}) \right\} - \ln Q \quad (1)$$

where  $\phi_R(\mathbf{r})$  and  $\phi_C(\mathbf{r})$  represent the monomer densities of rods and coils, respectively, and  $\omega_R(\mathbf{r})$  and  $\omega_C(\mathbf{r})$  are the chemical potential fields conjugated to the densities of rods and coils, respectively.  $\chi$  denotes the Flory-Huggins interaction parameter.  $\mathbf{M}(\mathbf{r})$  is the orientation field conjugated to the orientation order parameter  $\mathbf{S}(\mathbf{r})$ . Maier-Saupe interaction  $\mu N$  is used to represent the orientation interactions between the rods.<sup>64</sup>  $\eta(\mathbf{r})$  is used to enforce the incompressibility condition. The single chain partition function  $Q$  satisfies

$$Q = \frac{1}{V \int d\mathbf{u}} \int d\mathbf{u} \int d\mathbf{r} \exp \left[ - \int_0^{f_C} ds \Gamma(\mathbf{r} + \beta s \mathbf{u}, \mathbf{u}) \right] q_C(\mathbf{r}, f_C) \quad (2)$$

where  $q_C(\mathbf{r}, s)$  is the polymer segment probability distribution function representing the probability of finding the segment  $s$  ( $0 < s \leq f_C$ ) at position  $\mathbf{r}$  starting from the coil end ( $s = 0$ ). It satisfies a modified diffusion equation of a Gaussian chain model with the initial condition of  $q_C(\mathbf{r}, 0) = 1$ . Similarly,  $q_C^\dagger(\mathbf{r}, s)$  represents the probability for the segment  $s$  ( $0 < s \leq f_C$ ) starting from the rod-coil junction ( $s = f_C$ ) and ending at position  $\mathbf{r}$ .<sup>29,63</sup>

Minimizing the free energy functional with respect to  $\phi_R(\mathbf{r})$ ,  $\phi_C(\mathbf{r})$ ,  $\omega_R(\mathbf{r})$ ,  $\omega_C(\mathbf{r})$ ,  $\mathbf{S}(\mathbf{r})$ ,  $\mathbf{M}(\mathbf{r})$ , and  $\eta(\mathbf{r})$  leads to the following SCFT equations for rod-coil diblock copolymers

$$\omega_C(\mathbf{r}) = \chi N \phi_R(\mathbf{r}) + \eta(\mathbf{r}) \quad (3)$$

$$\omega_R(\mathbf{r}) = \chi N \phi_C(\mathbf{r}) + \eta(\mathbf{r}) \quad (4)$$

$$\phi_R(\mathbf{r}) + \phi_C(\mathbf{r}) = 1 \quad (5)$$

$$\phi_C(\mathbf{r}) = \frac{1}{Q} \int_0^{f_C} ds q_C(\mathbf{r}, s) q_C^\dagger(\mathbf{r}, s) \quad (6)$$

$$\phi_R(\mathbf{r}) = \frac{1}{Q \int d\mathbf{u}} \int_0^{1-f_C} ds \int d\mathbf{u} q_C(\mathbf{r} - \beta s \mathbf{u}, f_C) \\ \exp \left[ - \int_0^{1-f_C} ds \Gamma(\mathbf{r} - \beta \mathbf{u}(s - s'), \mathbf{u}) \right] \quad (7)$$

$$\mathbf{M}(\mathbf{r}) = \mu N \mathbf{S}(\mathbf{r}) \quad (8)$$

$$\mathbf{S}(\mathbf{r}) = \frac{1}{Q \int d\mathbf{u}} \int_0^{1-f_C} ds \int d\mathbf{u} q_C(\mathbf{r} - \beta s \mathbf{u}, f_C) \\ \exp \left[ - \int_0^{1-f_C} ds \Gamma(\mathbf{r} - \beta \mathbf{u}(s - s'), \mathbf{u}) \right] \left( \mathbf{u} \mathbf{u} - \frac{\mathbf{I}}{3} \right) \quad (9)$$

where  $\Gamma(\mathbf{r}, \mathbf{u})$  represents the external fields related to the density and orientation of the rods, which can be written as  $\Gamma(\mathbf{r}, \mathbf{u}) = \omega_R(\mathbf{r}) - \mathbf{M}(\mathbf{r}) : (\mathbf{u} \mathbf{u} - \frac{\mathbf{I}}{3})$ , where  $\mathbf{I}$  is a  $3 \times 3$  unit matrix and  $\mathbf{u}$  is a unit orientation vector of the rod block.

By numerically solving the above SCFT equations, the density distributions of the rigid and flexible segments can be obtained, namely, the self-assembled morphologies.<sup>65</sup> The orientation vector  $\mathbf{u}$  of the rods is considered in a spherical surface, which is discretized into icosahedron triangular meshes.<sup>66</sup> We use the pseudospectral method<sup>67</sup> to solve the diffusion equation for the flexible segments and calculate the density and orientation order parameters of the rigid rods in the Fourier space by using the fast Fourier transform.<sup>68</sup>

**String Method.** The string method may not be based on a preunderstanding of the dynamics of the system but rather based on the analysis of the free energy landscape, thus obtaining the minimum energy pathway (MEP) of the phase transitions.<sup>69–71</sup> Therefore, the string method can be combined with various tools that can obtain the free energy or its derivative on the string to jointly explore the dynamic characteristics of the system. Because of the advantages of the SCFT in the calculation of ordered phases and their free energies in block copolymers, it can be combined well with the string method to explore the free energy landscape.<sup>23,24</sup> The different phase structures with the minimum free energy calculated by SCFT can be used as the two ends of the string (set as M and N), and their free energies are  $F_M$  and  $F_N$ , respectively. The main purpose of the string method is to obtain the MEP between M and N in the given energy landscape. MEP is a curve connecting the two extremes of the free energy functional  $F$  in the conformation space, namely the string  $\tau$ , which satisfies the equation

$$(\nabla F)^\perp(\tau) = 0 \quad (10)$$

where  $(\nabla F)^\perp$  denotes the component of  $\nabla F$  perpendicular to the string  $\tau$ . The effect of the above equation is to make the free energy fall only in the direction perpendicular to the string. According to the improved string method proposed by E,<sup>71</sup> enforcing an equal arc length restriction, that is, ensuring the constant “distance” between each structure on the string to maintain the shape of the string, can prevent the structures on the string from falling into local minima during the convergence process and losing the information on the string. The realization in the computer program is that, after the iteration for a few steps in running the SCFT for each state on the string, regulation of the string using difference method or cubic spline interpolation is conducted. The procedures of iterating and regulating the string need to be repeated until convergence of the string evolution. The MEP connecting the two metastable states M and N is parametrized as  $\tau(\alpha)$  by a variable  $\alpha$  ( $\alpha \in [0,1]$ ). The implementation procedures of the string method are as follows:

Determine the two ends of the string. By the calculation of the SCFT, the two ends of the string  $\phi_M$  and  $\phi_N$  can be obtained, i.e., the extremum values by variations of  $F$  with respect to computation cell size and initial fields, corresponding to the stable or metastable structures of the system.

Discretize the string. Discretize the string  $\tau(\alpha)$  into  $n + 1$  points  $\{\phi_0, \phi_1, \phi_2, \dots, \phi_n\}$ . Each point represents a state (order parameter) of the system, and  $\tau(0) = \phi_M$ ,  $\tau(1) = \phi_N$  ( $\alpha = i/n$ ,  $i = 0, 1, 2, \dots, n$ ).

Initialize the string. According to the order parameters  $\phi_M$  and  $\phi_N$  of the corresponding structures at both ends of the string, the initial structures of each discrete point on the string are obtained by combining the two structures at the ends in different ways. Similar to the SCFT calculations, the string method is also very sensitive to the initial values.

In this article, the string is initialized by making the initial order parameter for each state evolve gradually along the string in the whole calculation cell

$$\phi_i(\mathbf{r}) = \phi_M(\mathbf{r}) + \frac{i}{n}(\phi_N(\mathbf{r}) - \phi_M(\mathbf{r})), \quad i = 0, 1, \dots, n \quad (11)$$

With this initialization method, when the final free energy barrier of the MEP is 0, the phase transitions proceed via spinodal decomposition; otherwise, the metastable structures obtained in the MEP can be considered as the intermediate states in the multistep nucleation and growth process.

Iterate and adjust the string. Each structure on the initial string is input as initial value in the SCFT followed by iterations (such as 5 time steps) and interpolation. The string needs to be iterated and adjusted repeatedly until it eventually converges to the MEP. The obtained MEP is indicated as the evolution of  $F - F_0$  along the string, i.e., the free-energy difference between the discretized states on the string and the initial state M.

Compared with the flexible block copolymer system, additional order parameters are required to describe the phases self-assembled by a chain rigidity-containing system: the density order parameter  $\phi_C(\mathbf{r})$  ( $\phi_R(\mathbf{r})$ ) and the orientation order parameter  $S(\mathbf{r})$  for rod blocks or the chemical potential field  $\omega_C(\mathbf{r})$  ( $\omega_R(\mathbf{r})$ ) and the orientation field  $M(\mathbf{r})$  for rod blocks that are conjugated with the order parameters. Therefore, in addition to the monomer density fields, the usually adopted equal arc length restrictions also need to be enforced on  $S(\mathbf{r})$  or  $M(\mathbf{r})$ . When the orientation interaction between rigid rods is small, the interpolation on  $S(\mathbf{r})$  or  $M(\mathbf{r})$  is not necessary. This is because the orientation degree of the rods can be very low and the orientation can be set as random initial fields, which has no effect on the calculation stability and can improve the calculation efficiency. However, at present we consider the equal length restriction to both density fields and orientation order parameter, mainly to avoid the unstable convergence process. In particular when the geometrical asymmetry effect  $\beta$  and the orientation interaction  $\mu N$  are large, random initial fields of the orientation are difficult to converge to the desired structures, and the calculation will become corrupted and fail to obtain the MEP.

There are two main challenges to the theoretical calculation of phase transitions in rod-coil diblock copolymers. First, the 3D self-assembled mesophases are still not sufficiently studied compared to the coil-coil blocks. At present, the SCFT algorithm for rod-coil block copolymers can only handle a narrower parameter space than that for flexible block copolymers. The convergence becomes poor and the calculation unstable under large values of  $\beta$  and  $\mu N$ . In this case, introducing the string method will increase the difficulty in numerical calculations. This is mainly due to the emergence of complex intermediate states (including various transient and metastable structures) with serious curvature variation. The rigid rods need to experience drastic changes and rearrangement within these complex structures along the string, which may lead to the extremely unstable calculation during the string evolution. Second, the nucleation issues are sidestepped in this article due to low computational efficiency for numerical treatment to rigid rods. This is because when we calculate the nucleation process, the calculation box must be large enough to ensure accurate shape and size of the critical nucleus and also must be in the 3D space to avoid confinement effect. However, a large computational box requires finer spatial resolution and thus reduces the computational efficiency. In this article, for calculation stability, we choose relatively small values of  $\beta$  and  $\mu N$ . We carry out the calculation in a single unit cell to increase the computational efficiency. Linear interpolation is used to generate the initial string with the two ends of the string as the known inputs. Although the current calculations cannot handle the

nucleation issue, the key information such as the metastable states, epitaxial relationship, and spinodal decomposition process can be analyzed during the phase transitions. To further improve computational efficiency, we employ multithreaded calculations.

### III. RESULTS AND DISCUSSION

To implement the inverse design of kinetic pathways, we first determine the two metastable networks, such as SG and SD, as the target structures. As OOT between distinct structures usually occurs following an appropriate epitaxial growth relationship via nucleation and growth (refer to our previous work<sup>24,62,72</sup>), we need to identify the initial structures that can undergo an epitaxial phase transition with the target structure. The investigation on OOT in flexible block copolymers has shown that the matching of reciprocal lattice vectors and matching of lattice periods are two key factors that determine the epitaxial relationship between two structures. Here, we first search for the structures (the two ends of the string) that match the target structure based on these two factors. After obtaining the phase transition pathways, we will further analyze the effects of geometrical asymmetry between the rigid and flexible segments and the liquid crystal behavior of the rigid rods on the epitaxial phase transition.

Each self-assembled structure in block polymers belongs to a specific space group, and different structures may belong to the same space group with similar or different reciprocal lattice vectors. For many known phases, space groups and reciprocal lattice vectors have been determined experimentally or theoretically. For example, in experiments, the primary scattering peaks of the O<sup>70</sup> network correspond to three reciprocal lattice vectors: (111), (022), and (004).<sup>73</sup> Erukhimovich's weak segregation theory identified the reciprocal lattice vector of the SG as {110}.<sup>74</sup> Jiang et al.<sup>75</sup> estimated the reciprocal lattice vectors of more structures based on the crystal structure factor table. Therefore, the reciprocal lattice vectors of different single networks can be obtained according to the existing theoretical research, experimental results, and lattice structure factors. Because the alternating network and the single network have the same space group and similar reciprocal lattice vectors, according to our previous research on the epitaxial growth relationship between alternating networks and lamellae in ABC triblock terpolymers,<sup>72</sup> we can also speculate the reciprocal lattice vector of corresponding single networks. For example, alternating gyroid (G<sup>A</sup>) and SG belong to the same space group I4<sub>1</sub>32. G<sup>A</sup> has an epitaxial relationship with the {110} lamellae, and the reciprocal lattice vector of SG is also {110}. Similarly, alternating diamond (D<sup>A</sup>) and SD both belong to the Fd̄3m space group. As D<sup>A</sup> has an epitaxial relationship with the {111} lamellae, we can speculate that the reciprocal lattice vector of SD is {111}.

Next, we search for the two initial structures corresponding to the two ends of the string that match the target structure. For rod-coil block copolymers, our recent work has calculated the phase diagram and found that, with low orientation interaction ( $\chi N = \mu N \leq 20$ ), the stable structures only include lamellae and cylinders (pucks), which are also easy to be experimentally observed.<sup>63</sup> On the basis of these theoretical calculations, we need to find lamellae or cylinders with suitable symmetry as the initial structures. Using the method of setting specific initial density fields in real space, we can construct lamellae with different crystallographic planes and cylinders with different crystallographic directions. By minimizing their

free energy with respect to the cubic box size, we can obtain their unit cell size. The lamellae and cylinders with the same unit cell size with the single networks can be seen from Table 1. In the selected parameters, the unit cell size of {110}

**Table 1.** Matching Relationship between Target Single Networks and Simple Phases in Rod–Coil Diblocks<sup>a</sup>

phase	reciprocal lattice vectors or lattice symmetry	unit cell size/ $R_g$
single gyroid (SG)	{110}	(3.6, 3.6, 3.6)
single diamond (SD)	{111}	(4.4, 4.4, 4.4)
lamellae (L)	{111} L	(4.4, 4.4, 4.4)
	{110} L	(3.6, 3.6, 3.6)
	{211} L	>4.4
cylinders (C)	$\langle 111 \rangle C^{HEX}$	(3.6, 3.6, 3.6)
	$C^{TET}$	<3.6

<sup>a</sup>With  $\chi N = 13$ ,  $\mu N = 13$ ,  $\beta = 2$ , and  $f_C = 0.65$ .

lamellae and  $\langle 111 \rangle$  hexagonally packed cylinders ( $C^{HEX}$ ) is the same as that of the SG; the unit cell size of {111} lamellae is the same as that of the SD. For comparison, we also calculated other lamellae and cylinders (tetragonally packed cylinders,  $C^{TET}$ ) with different symmetries, which do not have a unit-cell-size matching relationship with the target structures. Each crystallographic plane or crystallographic direction group contains various planes or directions. For example, the {110} crystallographic plane group includes 12 different planes: (110), (101), (011), (−110), (−101), (0−11) etc. The {111} crystallographic plane group includes 8 crystallographic planes. Therefore, a natural idea is to take advantage of the rearrangement of different lamellae or different cylinders belonging to the same symmetry group to obtain the single networks in the reordering transition pathways. In fact, the

reordering transition behavior between lamellae or cylinders has been observed in experiments.<sup>76,77</sup> Through continuous annealing, rearrangements of lamellae or cylinders with different orientations have been achieved in thin film confinement systems with lamellae or cylinders with different orientations coexisting in the transition process. It is expected that, in 3D space, the reordering transitions will be more complicated.

Using the string method, we can calculate the reordering transition pathways of lamellae or cylinders. It is shown from Figure 1a that the SG, as an intermediate metastable state, appears in the reordering transition pathway of lamellae with different crystallographic planes but the same {110} group, illustrating there is an epitaxial growth relationship between {110} lamellae and the SG. The obtained string presents a catenary shape, showing axisymmetric characteristics, indicating that the intermediate SG is relatively long-lived (the difference of the single chain free energy between the peak and the valley is  $6 \times 10^{-4} k_B T$ ). However, we notice that, although the optimal unit cell size of  $C^{HEX}$  with {111} crystallographic direction is the same as that of the SG, the latter does not appear in the reordering transition pathways of the former (Figure 1c–e). Increasing the length-to-diameter ratio of the rigid rod ( $\beta$ ), as shown in Figure 1c, d, and e, we find that the shape of the string changes from V-like shape to bell-like shape, indicating that the intermediate structure changes from a relatively stable structure (lamellae) to a relatively unstable structure (perforated lamellae, PL). These results show that the kinetic pathways on which the SG is encountered favor the reordering transition of lamellae rather than cylinders. Single networks, which are a kind of continuous structure, tend to extend throughout the whole lattice space. Compared with the lamellae, the density distribution of the cylinders in the unit cell space is more scattered and there are more independent

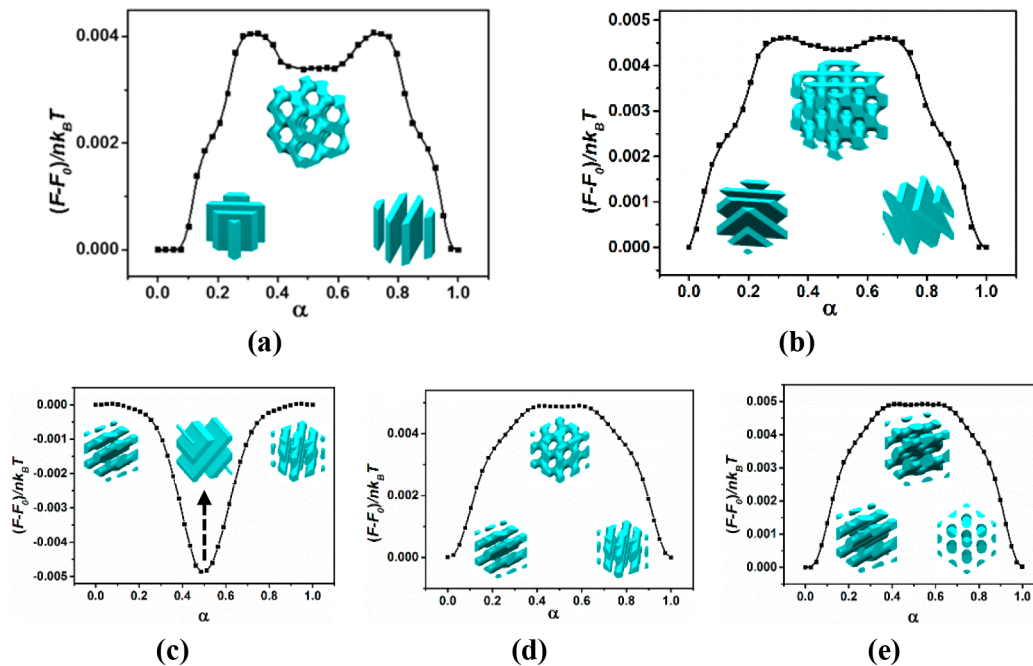


**Figure 1.** (a) Reordering transition pathway between {110} lamellae with single gyroid (SG) being encountered. (b) Reordering transition pathway between {111} lamellae with single diamond (SD) being encountered in rod–coil diblocks with  $\chi N = 13$ ,  $\mu N = 13$ ,  $\beta = 2$ , and  $f_C = 0.65$ . (c) Reordering transition pathway between {111} cylinders with {110} lamellae being encountered with  $\chi N = 13$ ,  $\mu N = 13$ ,  $f_C = 0.65$ , and  $\beta = 2$  (d) and (e) with  $\beta = 4$ .

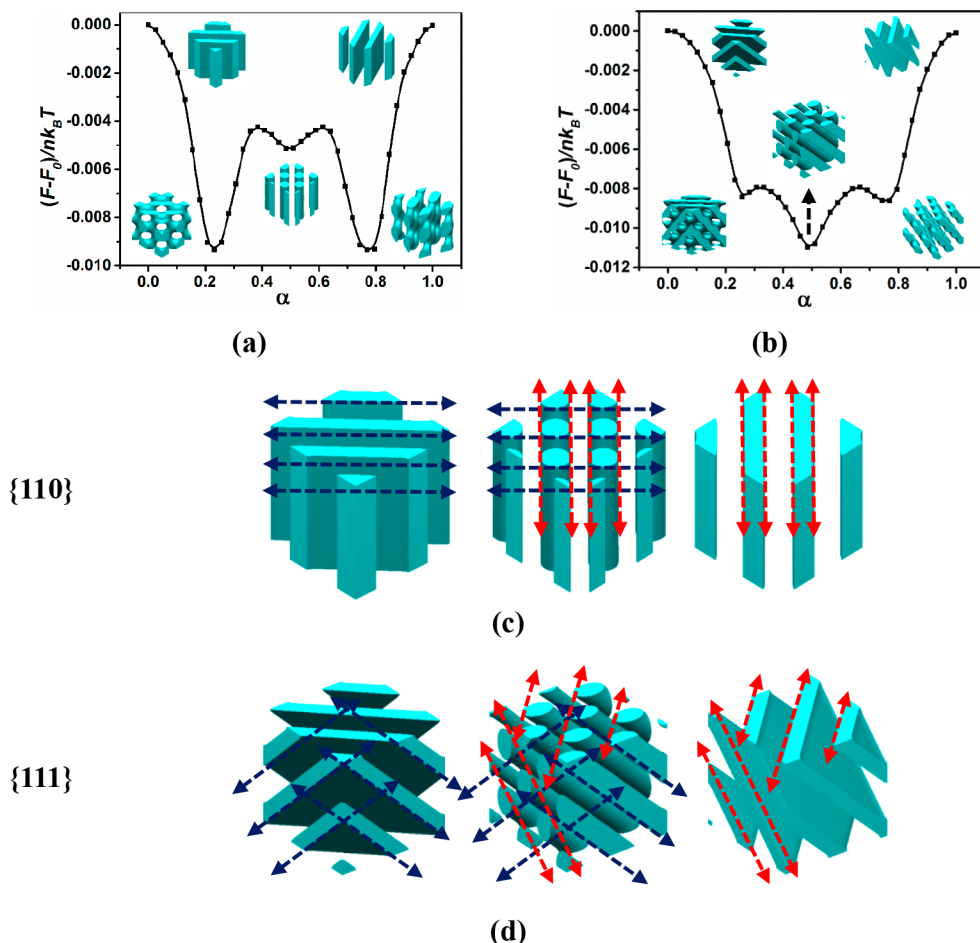


**Figure 2.** Reordering transition pathways (a) between  $\{110\}$  lamellae and (b) between  $\{111\}$  lamellae with  $\chi N = 13$ ,  $\mu N = 13$ ,  $\beta = 4$ , and  $f_C = 0.65$ . The metastable states corresponding to the valley of the MEP are shown as insets. The corresponding relationship of the overall position and orientation between the lamellae and the cylinders encountered in the reordering transition pathways are shown in (c) and (d), respectively. The blue and red dashed lines represent the corresponding relationship between the cylinders and the initial lamellae as well as between the cylinders and the terminal lamellae, respectively.

domains. Thus, it is more difficult for cylinders to rearrange to form a continuous network. In addition, we note that the shape of the strings shown in Figure 1d and e does not change, and the intermediate structures appearing in the phase transition pathways are both  $\{110\}$  PL. This indicates the reordering transition is not selective for the specific crystallographic orientation of two initial structures (two ends of the string), as long as they possess different orientations within the same symmetric group. Figure 1b shows the reordering transition pathway of the  $\{111\}$  lamellae, with SD network appearing in it as an intermediate metastable state. The shape of the string is similar to that in Figure 1a with the free energy barrier between the valley and the two peaks being  $2 \times 10^{-4} k_B T$ . It should be noted that the free energy barriers shown in this article are just for a single block copolymer. As we consider a system with volume  $V$  of  $n$  block copolymers, true energy barriers of the system, which includes all molecular chains, would be higher. However, because of the weak segregation strength ( $\chi N$ ), the fluctuation effect could not be ignored, which however is not considered in a mean field theory such as SCFT. In particular, when the free energy barriers for all molecular chains are relatively small, the system is extremely susceptible to thermal fluctuations. The effect of fluctuations on the phase behavior can be suppressed when polymer chains are long enough.<sup>24,78</sup>

Otherwise, the fluctuations may play a critical role and induce the phase transitions.<sup>19,20</sup>

On the basis of the analysis of the reciprocal lattice vectors and the lattice period, we have obtained the SG and SD networks using the method of inverse kinetic path design. However, the epitaxial phase transition of chain-rigidity-containing copolymers is affected by additional factors, mainly including the geometrical asymmetric effect between rigid and flexible block and the liquid crystal orientation effect of the rigid block. Comparing Figure 1a and b and Figure 2a and b, we can clearly see that increasing the conformational asymmetry effect, that is, making the rigid rods slender (from  $\beta = 2$  to  $\beta = 4$ ), induces the formation of cylinders in the kinetic pathways rather than single networks. The tetragonally packed cylinders ( $C^{TET}$ ) appear in the reordering transition pathways of  $\{110\}$  lamellae in Figure 2a, and the oblique hexagonally packed cylinders appear in the reordering transition pathways of  $\{111\}$  lamellae in Figure 2b. This is mainly due to the fact that slender rods are more difficult to rearrange on the kinetic pathways. In particular, when a complex network occurs in the reordering transition pathway, the structure curvature varies sharply during the phase transition process. According to previous quantitative analysis by Matsen and Bates,<sup>79</sup> the interfacial curvature increases as

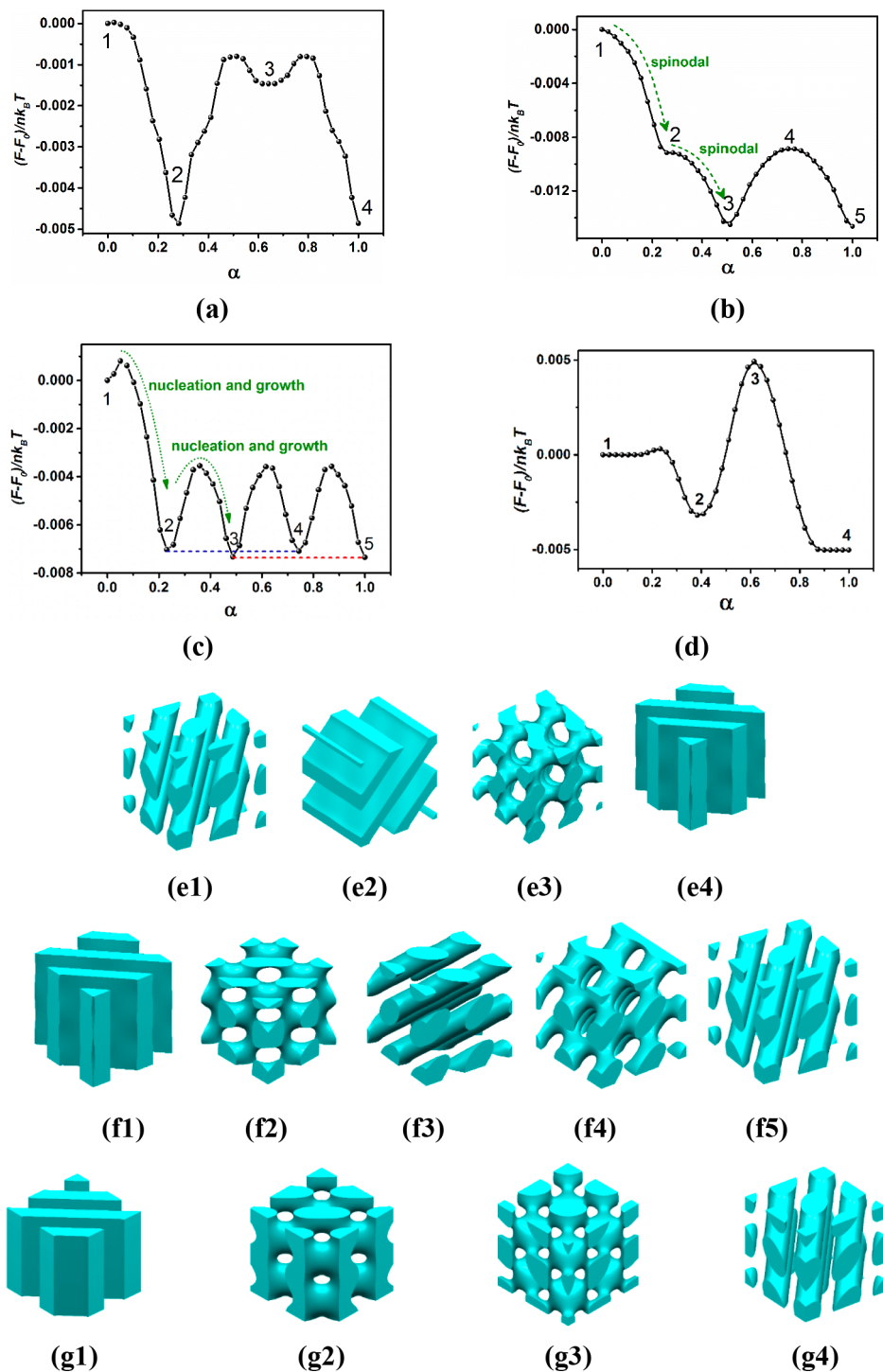


**Figure 3.** MEPs between  $\langle 110 \rangle$  lamellae and  $\langle 111 \rangle$  hexagonally packed cylinders ( $C^{HEX}$ ) in rod–coil diblocks with (a)  $\chi N = 13$ ,  $\mu N = 13$ ,  $\beta = 2$ , and  $f_C = 0.65$ . (b) Same parameters as (a) but  $\beta = 4$ , and (c) same parameters as (b) but  $f_C = 0.6$ . The characteristic structures in (a) indicated by numbers are shown in e1–e4, and the characteristic structures in (b) and (c) are shown in f1–f5. (e1-to-e2) and (f1-to-f3) are preferential phase transitions; (e2-to-e4) and (f3-to-f5) are reordering phase transitions. (d) MEP between  $\langle 110 \rangle$  lamellae and  $\langle 111 \rangle$  hexagonally packed cylinders ( $C^{HEX}$ ) in coil–coil diblocks with  $\chi N = 13$  and  $f = 0.6$ . The characteristic structures indicated by numbers are shown in g1–g4.

the self-assembled phases change from lamellae (with a flat interface) to other phases (with curved interfaces) and the curvature of the diamond and gyroid is higher than that of the PL. It is difficult for the slender rods to be readjusted to adapt to the change in curvature and form networks in the phase transition pathways. In this case, the rigid rods tend to preferentially form cylinders whose interfacial curvature is also

higher but overall orientation is similar to the initial lamellae. Panels c and d in Figure 2 show the correspondence of the overall orientation between the initial lamellae at the two ends of the rearrangement pathway and the intermediate cylinders. This correspondence avoids the large-scale migration of the slender rods within the unit cell in the phase transition process. It is worth noting that, with the selected parameters here, the

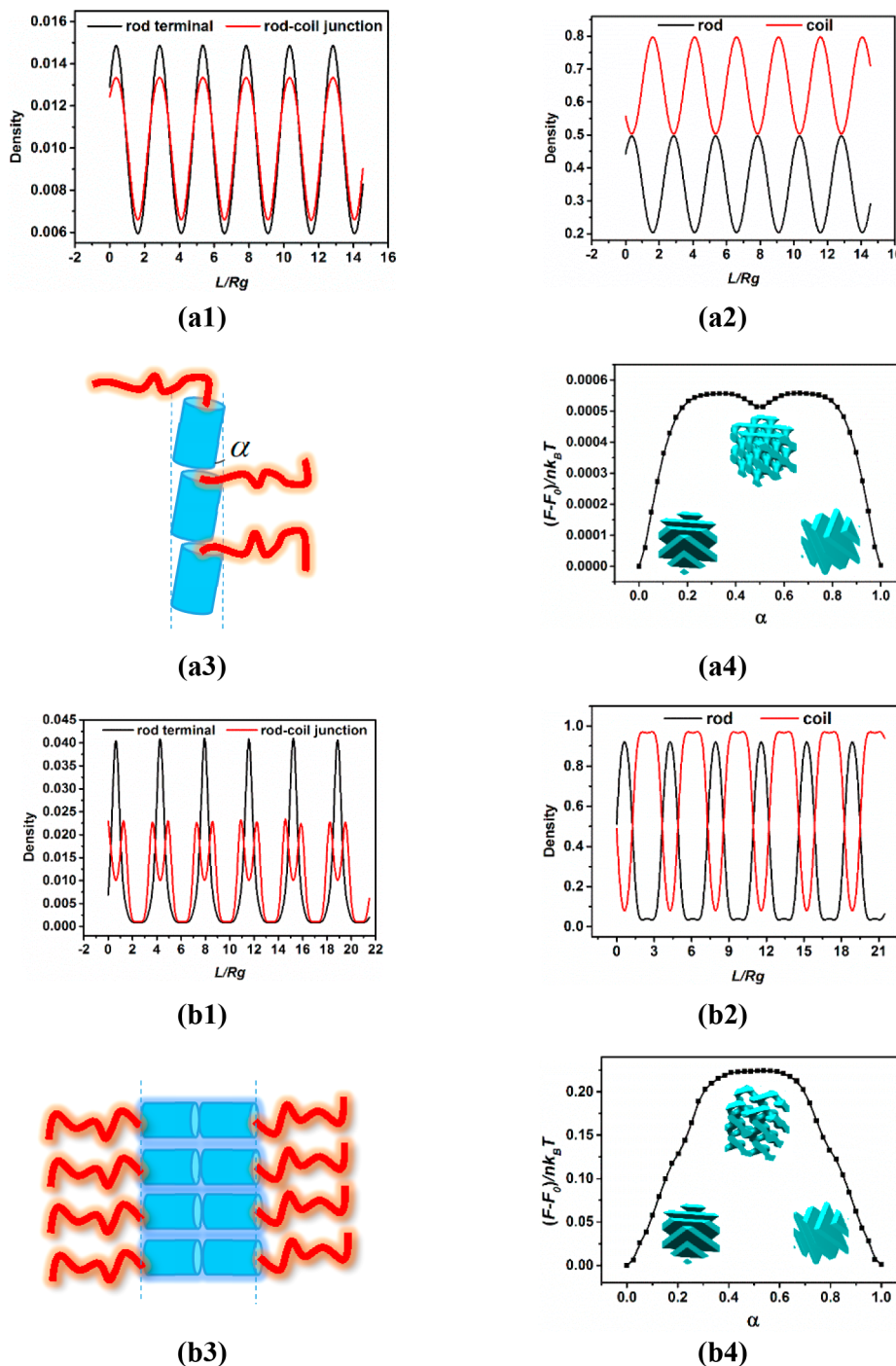


**Figure 4.** Rods within the  $\{111\}$  lamellae in  $\chi N = 12$ ,  $\mu N = 40$ ,  $\beta = 2$ , and  $f_C = 0.65$  can be arranged in two types: (a1–a3) show the  $\{111\}$  lamellae of type I with the density distributions of the rod terminal, rod–coil junction, and rod and coil blocks along the body diagonal as well as the illustration of the rod arrangement shown; (b1–b3) show the  $\{111\}$  lamellae of type II. The corresponding reordering transition pathways between  $\{111\}$  lamellae in type I and type II are shown in (a4) and (b4), respectively.

orientation degree of the rods is very low and does not form a good alignment driven by the orientation interaction. Despite this, the rigidity of the rods still prevents them from migrating drastically within the unit cell to form a complex network. On the other hand, slender rods generally undermine the formation of networks. When the orientation interactions are relatively large, the destructive effects are more pronounced and lead to the distortion or even destruction of the networked structure. Our following work will illustrate this issue in detail.

The lamellae with rods of larger aspect ratio ( $\beta = 4$ ) favor the priority phase transition into cylinders, therefore hindering the formation of single networks in the kinetic pathway. In our calculations, we find that priority phase transitions are very common in chain-rigidity containing systems, reflecting that chain rigidity can seriously influence the phase transition pathway. Herein, to further understand the characteristics of priority phase transitions, we display the lamellae–cylinder transitions.

As can be seen from Table 1, the  $\{110\}$  lamellae and the  $\{111\} C^{HEX}$  have the same lattice period. Therefore, epitaxial phase transition between these two structures may be achieved. Using the string method, we have obtained their phase transition pathway, as shown in Figure 3. It can be seen from Figure 3a that the  $\langle 111 \rangle C^{HEX}$  (e1) preferentially transforms into  $(101)$  lamellae (e2) through an extremely low free energy barrier, which then undergoes a reordering transition into  $(110)$  lamellae (e4). The SG (e3) is obtained in the reordering transition process, which is consistent with the above calculation results shown in Figure 1a. When the aspect ratio of the rods increases from  $\beta = 2$  to  $\beta = 4$ , the  $\langle 111 \rangle C^{HEX}$  becomes more stable than  $(110)$  lamellae. In this case, the phase transition from  $(110)$  lamellae to  $\langle 111 \rangle C^{HEX}$  also experiences the priority phase transition (Figure 3b). Namely, the  $(110)$  lamellae (f1) is preferentially transformed into a  $\langle 111 \rangle C^{HEX}$  (f3) with its overall orientation of the cylinders along the  $(110)$  plane;  $\langle 111 \rangle C^{HEX}$  (f3) is then rearranged to the target  $\langle 111 \rangle C^{HEX}$  (f5). The relatively unstable PL structure (f4) located at the peak is obtained, which is also consistent with the previous calculation results shown in Figure 1d and e. It can be seen from Figure 3b that the phase transition from f1 to f3 goes through a two-step spinodal decomposition process indicated by the green arrows. The multistep spinodal decomposition is similar to the multistep nucleation and growth reported by previous researchers.<sup>23</sup> However, in terms of the multistep spinodal decomposition, the phase transition process has no energy barrier, and the metastable structure (such as f2) encountered in the pathway does not have long-term stability. When the rod components increase (Figure 3c), the metastable structures that occur in the phase transition pathway remain the same, but their relative stability changes. The two-step spinodal decomposition (Figure 3b) becomes the two-step nucleation and growth process (Figure 3c). For comparison, we further calculate the phase transitions between the  $(110)$  lamellae and the  $\langle 111 \rangle C^{HEX}$  in coil-coil diblock copolymers, as shown in Figure 3d. Interestingly, the phase transition does not undergo the preferential transition and reordering transition. Instead, a single six-pronged network in Figure 3g3 appears in the transition pathway (although it is unstable), similar to our previous calculation in flexible ABC triblock terpolymers.<sup>72</sup> This network has six narrow branches around each bulky node, exhibiting serious packing frustration. In rod-coil diblock copolymers (Figure 3a–c), this single six-pronged network is not found in the phase transition pathways due to the priority phase transition. The priority phase transition in rod-coil diblocks is closely related to the rigidity of the rod blocks. Because the rods do not bend and the resulting internal conformational entropy is rather small, they are difficult to migrate in a large scale during the phase transition and thereby preferentially transform into structures with similar overall orientation to that of the initial structure. Because the rigid rods do not need to experience drastic rearrangement, the energy barrier during the priority phase transition is very low. In fact, the priority phase transition is similar to the principle that the matching of unit cell size determines the epitaxial relationship. If the starting and terminal structures have a large difference in the unit cell size, the phase transition requires long-distance movement and rearrangement of the molecules, and thus, the energy barrier is high.

The high orientation interaction between the rigid rods may induce parallel arrangement of the rods, resulting in liquid

crystal behavior and influencing the epitaxial phase transition. The parameter conditions  $\chi N = 12$ ,  $\mu N = 40$ ,  $\beta = 2$ , and  $f_C = 0.65$  are selected here to ensure the high orientation degree of the rods. By setting special orientation fields or orientation order parameters as the initial values, structures with different arrangement modes of rods in the parameter space can be obtained. Figure 4 shows two different arrangements of rods in the  $\{111\}$  lamellae. It is clear from Figure 4a1 and a2 that both the rod-coil junction and the rod terminal are located in the middle of the rod-rich domain for type I lamellae. According to the eigenvector  $\Lambda = [-0.1458 \ 0.9893 \ -0.0022]^T$  corresponding to the largest eigenvalue of  $S(r)$  in the region with the highest density of rods, the tilt angle  $\alpha$  of the rods is determined as  $8.39^\circ$  to the parallel direction of  $\{111\}$  lamellae. In the middle of the rod-rich domain, the coils are not expelled. Therefore, the rod orientation is almost parallel to the lamellae, as illustrated in Figure 4a3. In Figure 4b1, the rod-coil junction presents a two-peak distribution, whereas the rod terminal presents a single-peak distribution. The rods are parallel to the normal direction of  $\{111\}$  lamellae based on the eigenvector  $\Lambda = [0.00085 \ 0.00092 \ 1]^T$ . As the rod length is  $(1 - f_C) \times \beta = 0.7 R_g$ , two times the rod length projected in the normal direction of the lamellae can be calculated as  $0.7 R_g \times \cos 0^\circ \times 2 = 1.4 R_g$ . The distance between the two peaks of the density distribution for the rod-coil junction is  $1.33 R_g$ . Therefore, the lamellae shown in Figure 4b1–b3 are smectic-A phase with two-layer arrangement, which is indicated as type II. When the rod arrangement in the  $\{111\}$  lamellae is type I, the reordering transition pathway is shown in Figure 4a4 with SD encountered in this pathway. However, when the rod arrangement in the  $\{111\}$  lamellae is type II, SD does not occur in the phase transition pathway. Instead, a perforated discontinuous structure appears, which is an unstable state (Figure 4b4). When calculating the phase transition of the lamellae in type II, we find the calculation stability becomes worse. It can also be seen from the string shape that the string appears to be a little distorted and that the symmetry of its overall shape deteriorates. This shows the rearrangement process of the lamellae in type II is more difficult. Comparing the single chain free energy barriers of the two phase transition pathways, we find that the energy barrier to be overcome during the phase transition of lamellae in type II ( $10^{-1}$ ) is 3 orders of magnitude higher than that of lamellae in type I ( $10^{-4}$ ), which can account for the more difficult phase transition in type II.

The overall degree of orientational order of the rod segments can be quantified according to the order parameter  $\tilde{S}(r) = 3/2 \times \lambda_{max}(r)$ , where  $\lambda_{max}(r)$  represents the maximum eigenvalue of the matrix tensor  $S(r)$ .<sup>29</sup>  $\tilde{S}(r) = 1$  and  $\tilde{S}(r) = 0$  indicate that the rod segments are completely aligned and have poor orientation, respectively. In terms of the two types of lamellae shown in Figure 4, we find that the orientation degree of the rod segments in type I is very low ( $\tilde{S}(r) = 0.0042$ ), whereas that in type II is much higher ( $\tilde{S}(r) = 0.798$ ). It can be seen from Table 2 that, for lamellae in type I, the orientation degree of the rigid rods is rather low (<0.005) regardless of the orientation interaction and that no liquid crystal orientation effect occurs. The lamellae in type II (double-layer smectic-A) display liquid crystal behavior and appear only when the orientation interaction is high. For example, we have discovered the lamellae in type II at  $\mu N = 32$ , 36, and 40, where the orientation degree of the rod segments is 0.657, 0.752, and 0.798, respectively, much higher than that in type I.

**Table 2. Orientation Degree ( $\tilde{S}(r)$ ) and Direction ( $\alpha$ ) of the Rod Segments and Different Energy Contributions (Interfacial Energy  $F_{\text{inter}}$ , Entropic Energy  $-TS$ , and Orientation Interaction Energy  $F_{\text{orien}}$ ) of the Lamellae in Type I in Different Orientation Interactions ( $\mu N$ )**

$\mu N$	$\tilde{S}(r)$	$\alpha$	$F_{\text{inter}}$	$-TS$	$F_{\text{orien}}$
12	0.0008	9.0°	95.05%	4.95%	0
24	0.0014	9.0°	95.02%	4.98%	0
28	0.0017	9.0°	95.02%	4.98%	0
32	0.0021	8.85°	95.00%	4.99%	0.01%
36	0.0029	8.47°	94.99%	5.00%	0.01%
40	0.0042	8.39°	94.96%	5.03%	0.01%

The rod segments with high orientation degree and orderly arrangement favor an interface with zero curvature, and thus it is difficult to induce the formation of complex multibranched and high-curvature network structures. Therefore, the low orientation degree in type I creates a convenient condition for forming a network structure in the phase transition pathway. From Figure 5, the rigid rods in the branches of the SD network are basically arranged along the direction in which the branches extend, exhibiting a small angle offset, but the degree of overall orientation is low (<0.005), that is, the rigid rods are arranged with a number of defects. At the network nodes, the rigid rods arranged in different directions in each network branch meet each other to make the rod arrangement much more disordered, and the orientation degree is even lower than that in network branches. The low orientation degree of the

rigid segments in the lamellae in type I makes it possible to pack the rigid rods at the nodes of the multibranch network, and the high liquid crystal orientation effect in type II induces high packing frustration to form networks. In other words, there is a serious steric problem to pack the rods in parallel and orderly into the network nodes. Therefore, it is difficult to form a network structure in the reordering transition pathway between the lamellae in type II.

From the perspective of different energy contributions, we can further understand the differences in the reordering transition pathways with the two arrangement modes. According to different energy contributions of the lamellae in type I shown in Table 2, we can notice that the ratios of the interfacial energy in different orientation interactions are all ~95% and that the orientation interaction energy makes almost no contribution to the structure formation. Taking  $\mu N = 32$  as an example, we try to compare the contribution of different energies in the lamellae in type I and type II. For the lamellae in type I, the interfacial energy, entropic energy, and orientation interaction energy account for 95, 4.99, and 0.01%, respectively. The proportions of these three energies in the lamellae in type II are 58.84, 4.27, and 36.89%, respectively. The higher orientation interaction energy in type II ensures that the rigid rods can be arranged in parallel. This hinders the formation of the network structure during the phase transition process, which needs the destruction of the ordered arrangement, especially at the network nodes. In addition, the high interfacial energy in the lamellae in type I is beneficial to the transformation into the network structure, which has high

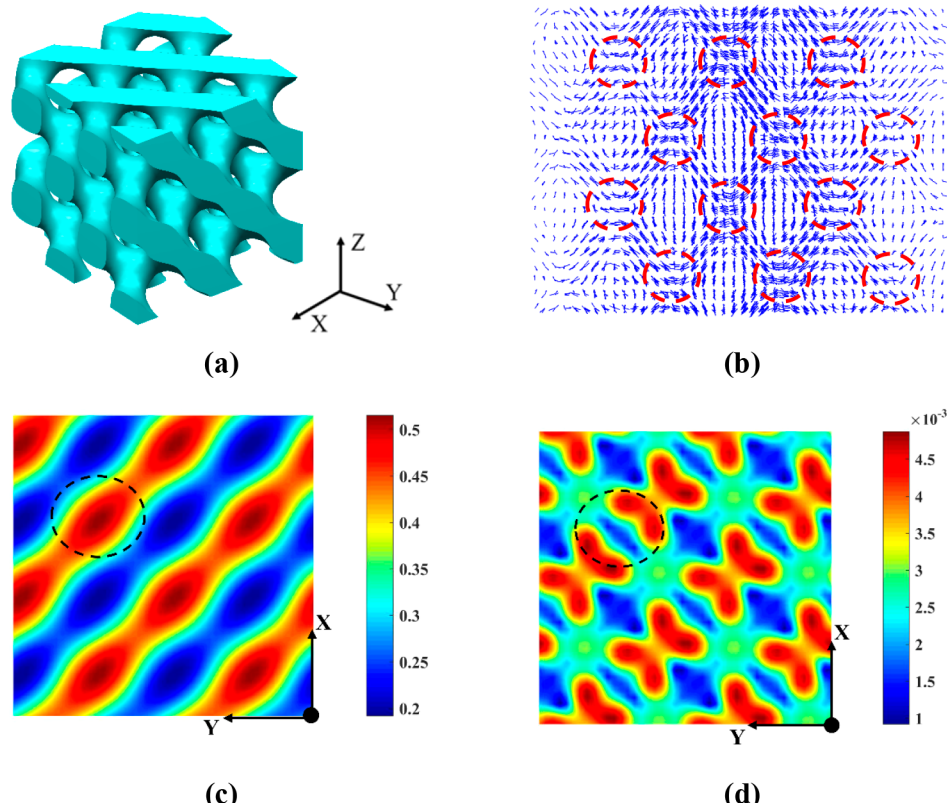


**Figure 5.** (a) The 3D morphology of the rod-forming SD obtained in the reordering transition pathway between  $\{111\}$  lamellae in type I when  $\mu N = 40$ . (b) Visualization of tensor field  $S(r)$  along the  $[110]$  crystallographic direction, illustrating the local preferred orientation direction of rod blocks. (c) The 2D density profile for the rod blocks from the top view of (a). (d) The orientation degree of the rod segments corresponding to the density profiles in (c). Both the black and red dashed circles in the above figures indicate the location of the network nodes.

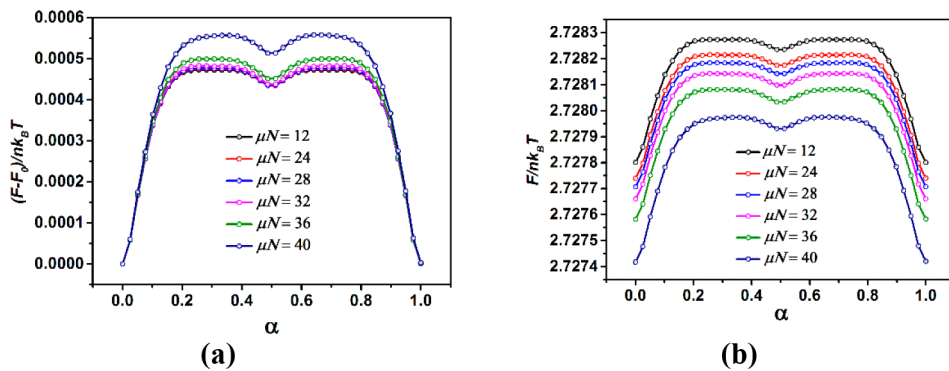


**Figure 6.** (a) Reordering transition pathways between {111} lamellae of type I in different orientation interactions. For clarity, we use the free energy ( $F$ ) of different states on the string instead of the free-energy difference ( $F - F_0$ ) between different states and the starting state to indicate the MEPs, which are shown in (b).

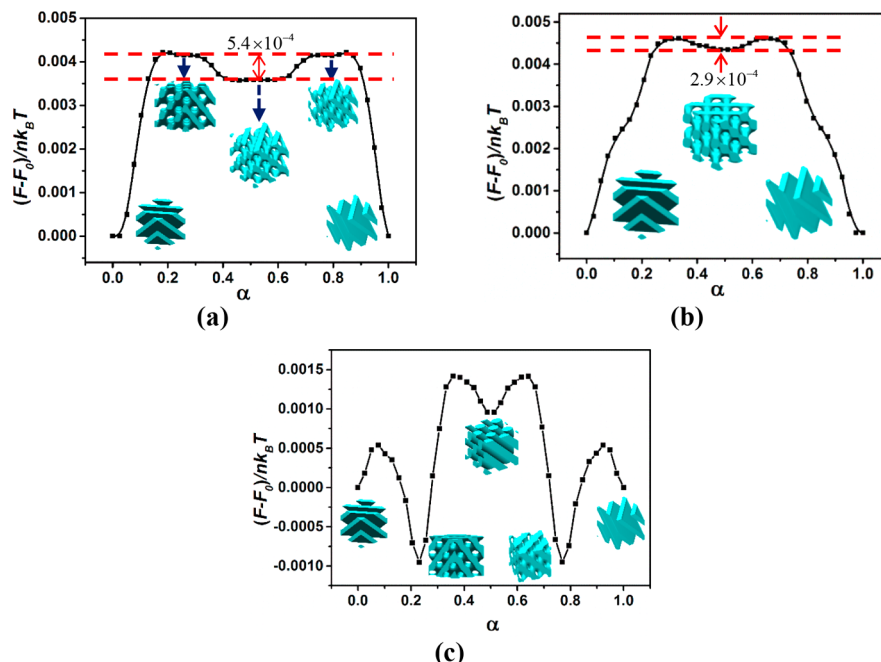


**Figure 7.** Effect of  $\beta$  on the reordering transition pathways of {111} lamellae in rod–coil blocks with  $\chi N = 13$ ,  $\mu N = 13$ , and  $f_C = 0.65$  for  $\beta =$  (a) 1, (b) 2, and (c) 3.

interfacial area (interfacial energy up to 95.84%). It seems that there is little difference in the proportion of entropic energy contribution between the two arrangements. However, the orientation interaction energy in type I is actually negligible, and the ratio of the entropic energy to the interfacial energy is 0.05. In the type II arrangement, the ratios of the entropic energy to the interfacial energy and to the orientation interaction energy are 0.07 and 0.12, respectively. Therefore, the contribution of the entropic energy to the formation of the lamellae in type II is greater than that in type I. In other words, the stretching of the flexible blocks in the lamellae of type II is more serious, and their movement is more limited compared to that of type I. Therefore, it is more difficult for the lamellae of type II to transform into a network structure by adjusting the molecular chains.

Figure 6 shows the MEPs of the reordering transition between the {111} lamellae in type I with different orientation interactions. The SD structure is encountered in all of these pathways, located in the intermediate valleys. The free energy barriers for a single chain between the valleys and the peaks of

the MEP in different orientation interactions are  $\sim 0.0004 k_B T$ , indicating that the orientation interaction does not affect the long-term stability of the SD obtained in the reordering transition pathway. Because the single networks self-assembled by block copolymers are metastable, they are difficult to be observed in experiments. Therefore, taking SD as an example, we expect to obtain the SD with long-term stability by regulating the kinetic pathway.

Figure 2b has shown that the increase in  $\beta$  leads to the disappearance of SD in kinetic pathways. Here, we will further investigate the effect of  $\beta$  on the long-term stability of SD in the reordering transition pathways of {111} lamellae. From Figure 7, as the asymmetric effect ( $\beta$ ) reaches  $\beta = 3$ , the SD just disappears in the reordering transition pathway. Comparing the free energy barriers of single chains marked in Figure 7a and b, we find that, when  $\beta = 1$ , which means the rods are very podgy and basically similar to nanoparticles, the SD needs to overcome higher energy barrier for a single chain ( $5.4 \times 10^{-4} k_B T$ ) to transform into other structures. It is proven here

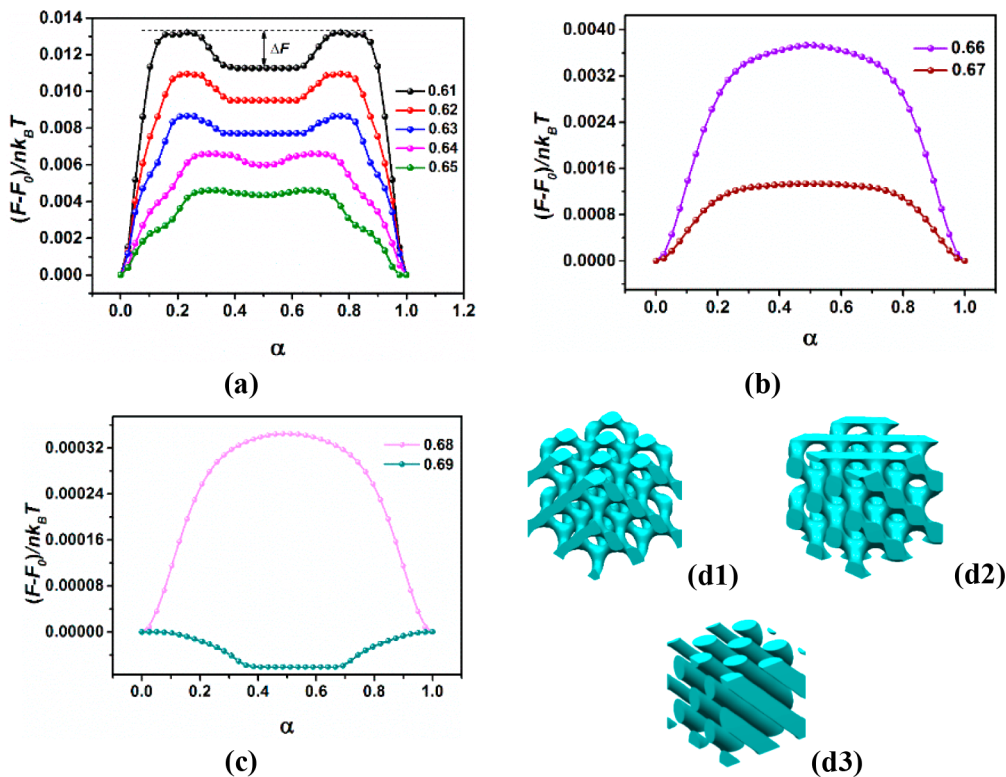


**Figure 8.** (a–c) Effect of coil fraction  $f_C$  on the reordering transition pathways of  $\{111\}$  lamellae in rod–coil blocks with  $\chi N = 13$ ,  $\mu N = 13$ , and  $\beta = 2$ . (d1) Intermediate metastable state (single diamond-like phase) at  $\alpha = 0.5$  of the MEP with  $f_C = 0.61$ – $0.63$ ; (d2) intermediate metastable state (single diamond phase) at  $\alpha = 0.5$  of the MEP with  $f_C = 0.64$  and  $0.65$ , and (d3) intermediate phase (oblique cylinders) at  $\alpha = 0.5$  of the MEP with  $f_C = 0.66$ – $0.69$ .

that the short and thick rods contribute to the long-term stability of complex network structures in the kinetic pathway.

Figure 8 and Table 3 show the influence of the block composition on the long-term stability of the intermediate SD

**Table 3. Effect of the Block Composition in Rod–Coil Diblocks on the Long-Term Stability of the Intermediate Structure in the Phase Transition Pathways**

coil fraction ( $f_C$ )	intermediate structure ( $\alpha = 0.5$ )	$F_1/k_B T$	$\Delta F/k_B T$
0.61	SD-like	0.0132	0.0019
0.62	SD-like	0.0110	0.0015
0.63	SD-like	0.0087	0.0010
0.64	SD	0.0066	0.0006
0.65	SD	0.0046	0.0002
0.66	cylinders	0.0037	not exist
0.67	cylinders	0.0013	not exist
0.68	cylinders	0.00035	not exist
0.69	cylinders	0	0.000061

in the phase transition pathway. With the increase of the rigid composition, there is a critical composition ( $f_C = 0.65$ ) where the oblique cylinders ( $\alpha = 0.5$ ) in the reordering transition pathways disappear while the SD emerges. Further increasing the rigid composition, there is another critical composition ( $f_C = 0.63$ ) where the intermediate structure in the pathways changes from SD to SD-like structure. Both the SD and SD-like structures are single networks with 4-fold connector, whereas the connectors in the SD-like network are a little distorted. As the coil fraction decreases from  $f_C = 0.65$  to  $f_C = 0.61$ , the single-chain free energy barrier between the

intermediate single network in the valley and the two structures at the peaks gradually increases, indicating that the long-term stability of the intermediate structure increases. Two characteristic free energy barriers are defined here. One is the single-chain free energy barrier  $F_1$  beyond which the intermediate structure can be formed and the other is the single-chain free energy difference  $\Delta F$  between the valley and the two peaks. These two energy barriers of different block compositions are shown in Table 3. It is clear that the block composition has a significant influence on the long-term stability of the intermediate structure in kinetic pathways. The  $\Delta F$  in the case of  $f_C = 0.61$  is approximately an order of magnitude larger than that in  $f_C = 0.65$ . The increase in rigid composition makes it necessary for the  $\{111\}$  lamellae overcoming a higher energy barrier to form SD, but at the same time, the resulting SD becomes a long-lived structure in the kinetic pathway. It should be pointed out that the long-term stability of the metastable state is a kind of relative stability that is related to the phase transition path on which the metastable state is obtained. According to Table 3, we compare the single-chain energy barrier  $F_1$  with  $\Delta F$  and regard the intermediate structure as a long-lived metastable structure when it satisfies  $\Delta F \geq 1/10 \times F_1$ . According to this criterion, the SD can be considered as long-lived when  $f_C \leq 0.63$ . As we know, OOT between different phases usually proceeds epitaxially via nucleation and growth.<sup>19,20,24,62,72</sup> Because of computational limitations, we are currently unable to calculate the nucleation barrier, which requires large computational boxes to avoid critical nuclear confinement. However, according to our previous research on flexible block copolymer systems,<sup>24,62</sup> the variation trend of nucleation barriers is the

same as that of the barriers obtained by linear interpolation method used in this article, so we can evaluate the former based on the latter.

The reordering transitions in experiments are usually activated by continuous annealing<sup>76,77</sup> and the orientation of the initial structure can be controlled by modified substrates. Thermal annealing may not enable the initial structure to transform into another one with an expected symmetry. However, this may be achieved by exerting external fields such as flow field, magnetic field, pressure field, and electric field along the appropriate direction (for example, along the orientation direction of the terminal structure). In fact, a real phase transition process is subjected to various processing conditions.<sup>1,9</sup> The importance is how they can be regulated to satisfy desired intensity and direction. We hope to conduct more investigations about the effect of external fields on phase transitions in the future.

#### IV. CONCLUSIONS

In the current work, the string method is applied to the SCFT of rod-coil diblock copolymers to establish a theoretical method for investigating the phase transition kinetics of chain rigidity-containing block copolymers. The existence of chain rigidity mainly produces two effects: geometrical asymmetry between rigid and flexible segments as well as the liquid crystal orientation effect of the rigid segments. The first effect (also indicating the shape of the rod) affects the variety and long-term stability of the metastable structure in the phase transition pathway. Compared with the flexible block copolymers, the chain rigid-containing systems are more likely to undergo a priority phase transition to avoid the large-scale rearrangement of the molecules. This phase transition priority will lead to difficulty in undergoing drastic concentration exchange during the phase transition process and in forming complex network structures. The liquid crystal behavior of the rigid rods makes the epitaxial phase transition relate closely to the arrangement manner of the rods. In summary, compared to the flexible block copolymer systems, the larger parameter space in chain rigidity-containing systems requires more precise control of the phase transition pathways to achieve the fabrication of target structures.

We use rod-forming single networks as the target structures and develop an inverse design strategy of phase transition pathways. The initial structures with designed specific symmetry connecting the kinetic pathway are lamellae or cylinders (pucks) that can be easily observed in experiments. By regulating the parameter space, it is expected to achieve the fabrication of long-lived single networks. The method we developed can be used to investigate the kinetic pathways to more complex self-assembled mesophases, especially those metastable states controlled by a kinetic process. Thus, the results may contribute to engineering complex nanostructures via designed kinetic routes.

#### AUTHOR INFORMATION

##### Corresponding Author

\*E-mail: [pingtang@fudan.edu.cn](mailto:pingtang@fudan.edu.cn).

##### ORCID

Ping Tang: [0000-0003-0253-1836](https://orcid.org/0000-0003-0253-1836)

##### Notes

The authors declare no competing financial interest.

#### ACKNOWLEDGMENTS

We are thankful for financial support from the National Natural Science Foundation of China (Grants 21574027, 21774027, and 21534002).

#### REFERENCES

- (1) Bates, C. M.; Bates, F. S. 50th Anniversary Perspective: Block Polymers—Pure Potential. *Macromolecules* **2017**, *50*, 3–22.
- (2) Müller, M.; de Pablo, J. J. Computational Approaches for the Dynamics of Structure Formation in Self-Assembling Polymeric Materials. *Annu. Rev. Mater. Res.* **2013**, *43*, 1–34.
- (3) Sun, D.-W.; Müller, M. Process-Accessible States of Block Copolymers. *Phys. Rev. Lett.* **2017**, *118*, 067801.
- (4) Forster, S.; Khandpur, A. K.; Zhao, J.; Bates, F. S.; Hamley, I. W.; Ryan, A. J.; Bras, W. Complex Phase-Behavior of Polyisoprene-Polystyrene Diblock Copolymers near the Order-Disorder Transition. *Macromolecules* **1994**, *27*, 6922–6935.
- (5) Imai, M.; Sakai, K.; Kikuchi, M.; Nakaya, K.; Saeki, A.; Teramoto, T. Kinetic Pathway to Double-Gyroid Structure. *J. Chem. Phys.* **2005**, *122*, 214906.
- (6) Hamley, I. W.; Fairclough, J. A.; Ryan, A. J.; Mai, S.; Booth, C. Lamellar-to-Gyroid Transition in a Poly (Oxyethylene)-Poly (Oxybutylene) Diblock Copolymer Melt. *Phys. Chem. Chem. Phys.* **1999**, *1*, 2097–2101.
- (7) Sakurai, S.; Umeda, H.; Furukawa, C.; Irie, H.; Nomura, S.; Lee, H. H.; Kim, J. K. Thermally Induced Morphological Transition from Lamella to Gyroid in a Binary Blend of Diblock Copolymers. *J. Chem. Phys.* **1998**, *108*, 4333–4339.
- (8) Hajduk, D. A.; Takenouchi, H.; Hillmyer, M. A.; Bates, F. S.; Vigild, M. E.; Almdal, K. Stability of the Perforated Layer (PL) Phase in Diblock Copolymer Melts. *Macromolecules* **1997**, *30*, 3788–3795.
- (9) Cochran, E. W.; Bates, F. S. Shear-Induced Network-to-Network Transition in a Block Copolymer Melt. *Phys. Rev. Lett.* **2004**, *93*, 087802.
- (10) Kim, K.; Schulze, M. W.; Arora, A.; Lewis, R. M.; Hillmyer, M. A.; Dorfman, K. D.; Bates, F. S. Thermal Processing of Diblock Copolymer Melts Mimics Metallurgy. *Science (Washington, DC, U. S.)* **2017**, *356*, 520.
- (11) Chu, C.-Y.; Lin, W.-F.; Tsai, J.-C.; Lai, C.-S.; Lo, S.-C.; Chen, H.-L.; Hashimoto, T. Order–Order Transition between Equilibrium Ordered Bicontinuous Nanostructures of Double Diamond and Double Gyroid in Stereoregular Block Copolymer. *Macromolecules* **2012**, *45*, 2471–2477.
- (12) Seddon, A. M.; Hallett, J.; Beddoes, C.; Plivelic, T. S.; Squires, A. M. Experimental Confirmation of Transformation Pathways between Inverse Double Diamond and Gyroid Cubic Phases. *Langmuir* **2014**, *30*, 5705–5710.
- (13) Oka, T. Transformation between Inverse Bicontinuous Cubic Phases of a Lipid from Diamond to Gyroid. *Langmuir* **2015**, *31*, 11353–11359.
- (14) Oka, T. Transformation between Inverse Bicontinuous Cubic Phases of a Lipid from Diamond to Primitive. *Langmuir* **2015**, *31*, 3180–3185.
- (15) Squires, A. M.; Templer, R. H.; Seddon, J. M.; Woenkhaus, J.; Winter, R.; Narayanan, T.; Finet, S. Kinetics and Mechanism of the Interconversion of Inverse Bicontinuous Cubic Mesophases. *Phys. Rev. E* **2005**, *72*, 011502.
- (16) Bates, F. S.; Hillmyer, M. A.; Lodge, T. P.; Bates, C. M.; Delaney, K. T.; Fredrickson, G. H. Multiblock Polymers: Panacea or Pandora's Box? *Science* **2012**, *336*, 434–440.
- (17) Tyler, C. A.; Morse, D. C. Orthorhombic Fddd Network in Triblock and Diblock Copolymer Melts. *Phys. Rev. Lett.* **2005**, *94*, 208302.
- (18) Tyler, C. A.; Qin, J.; Bates, F. S.; Morse, D. C. SCFT Study of Nonfrustrated ABC Triblock Copolymer Melts. *Macromolecules* **2007**, *40*, 4654–4668.
- (19) Matsen, M. W. Cylinder ↔ Gyroid Epitaxial Transitions in Complex Polymeric Liquids. *Phys. Rev. Lett.* **1998**, *80*, 4470–4473.

- (20) Matsen, M. W. Cylinder↔Sphere Epitaxial Transitions in Block Copolymer Melts. *J. Chem. Phys.* **2001**, *114*, 8165–8173.
- (21) Wickham, R. A.; Shi, A.-C.; Wang, Z.-G. Nucleation of Stable Cylinders from a Metastable Lamellar Phase in a Diblock Copolymer Melt. *J. Chem. Phys.* **2003**, *118*, 10293–10305.
- (22) Wang, C.; Jiang, K.; Zhang, P.; Shi, A.-C. Origin of Epitaxies between Ordered Phases of Block Copolymers. *Soft Matter* **2011**, *7*, 10552–10555.
- (23) Cheng, X.; Lin, L.; E, W.; Zhang, P.; Shi, A.-C. Nucleation of Ordered Phases in Block Copolymers. *Phys. Rev. Lett.* **2010**, *104*, 148301.
- (24) Ji, N.; Tang, P.; Qiu, F.; Shi, A.-C. Kinetic Pathways of Lamellae to Gyroid Transition in Weakly Segregated Diblock Copolymers. *Macromolecules* **2015**, *48*, 8681–8693.
- (25) Takahashi, H.; Laachi, N.; Delaney, K. T.; Hur, S.-M.; Weinheimer, C. J.; Shykind, D.; Fredrickson, G. H. Defectivity in Laterally Confined Lamella-Forming Diblock Copolymers: Thermodynamic and Kinetic Aspects. *Macromolecules* **2012**, *45*, 6253–6265.
- (26) Müller, M.; Smirnova, Y. G.; Marelli, G.; Fuhrmans, M.; Shi, A.-C. Transition Path from Two Apposed Membranes to a Stalk Obtained by a Combination of Particle Simulations and String Method. *Phys. Rev. Lett.* **2012**, *108*, 228103.
- (27) Li, W.; Müller, M. Thermodynamics and Kinetics of Defect Motion and Annihilation in the Self-Assembly of Lamellar Diblock Copolymers. *Macromolecules* **2016**, *49*, 6126–6138.
- (28) Li, W.; Nealey, P. F.; de Pablo, J. J.; Müller, M. Defect Removal in the Course of Directed Self-Assembly Is Facilitated in the Vicinity of the Order-Disorder Transition. *Phys. Rev. Lett.* **2014**, *113*, 168301.
- (29) Pryamitsyn, V.; Ganeshan, V. Self-Assembly of Rod–Coil Block Copolymers. *J. Chem. Phys.* **2004**, *120*, 5824–5838.
- (30) Tang, J.; Jiang, Y.; Zhang, X.; Yan, D.; Chen, J. Z. Y. Phase Diagram of Rod–Coil Diblock Copolymer Melts. *Macromolecules* **2015**, *48*, 9060–9070.
- (31) Jiang, Y.; Chen, J. Z. Y. Influence of Chain Rigidity on the Phase Behavior of Wormlike Diblock Copolymers. *Phys. Rev. Lett.* **2013**, *110*, 138305.
- (32) Gao, J.; Tang, P.; Yang, Y. Non-Lamellae Structures of Coil–Semiflexible Diblock Copolymers. *Soft Matter* **2013**, *9*, 69–81.
- (33) Gao, J.; Song, W.; Tang, P.; Yang, Y. Self-Assembly of Semiflexible Block Copolymers: 2D Numerical Implementation of Self-Consistent Field Theory. *Soft Matter* **2011**, *7*, 5208.
- (34) Song, W.; Tang, P.; Zhang, H.; Yang, Y.; Shi, A.-C. New Numerical Implementation of Self-Consistent Field Theory for Semiflexible Polymers. *Macromolecules* **2009**, *42*, 6300–6309.
- (35) Morse, D. C.; Fredrickson, G. H. Semiflexible Polymers near Interfaces. *Phys. Rev. Lett.* **1994**, *73*, 3235.
- (36) Cai, Y.; Zhang, P.; Shi, A.-C. Liquid Crystalline Bilayers Self-Assembled from Rod–Coil Diblock Copolymers. *Soft Matter* **2017**, *13*, 4607–4615.
- (37) Zhang, X.; Wang, L.; Zhang, L.; Lin, J.; Jiang, T. Controllable Hierarchical Microstructures Self-Assembled from Multiblock Copolymers Confined in Thin Films. *Langmuir* **2015**, *31*, 2533.
- (38) Zhu, X.; Wang, L.; Lin, J. Self-Assembly of Rod–Coil Multiblock Copolymers: A Strategy for Creating Hierarchical Smectic Structures. *J. Phys. Chem. B* **2013**, *117*, 5748.
- (39) Park, J. W.; Thomas, E. L. Multiple Ordering Transitions: Hierarchical Self-Assembly of Rod–Coil Block Copolymers. *Adv. Mater.* **2003**, *15*, 585–588.
- (40) Olsen, B. D.; Shah, M.; Ganeshan, V.; Segalman, R. A. Universalization of the Phase Diagram for a Model Rod–Coil Diblock Copolymer. *Macromolecules* **2008**, *41*, 6809–6817.
- (41) Halperin, A. Smectic A-Smectic C Transition in Lamellae Formed by Rod–Coil Copolymers. *EPL (Europhysics Letters)* **1989**, *10*, 549.
- (42) Matsen, M. W.; Barrett, C. Liquid-Crystalline Behavior of Rod–Coil Diblock Copolymers. *J. Chem. Phys.* **1998**, *109*, 4108–4118.
- (43) McCulloch, B.; Portale, G.; Bras, W.; Pople, J. A.; Hexemer, A.; Segalman, R. A. Dynamics of Magnetic Alignment in Rod–Coil Block Copolymers. *Macromolecules* **2013**, *46*, 4462–4471.
- (44) McCulloch, B.; Portale, G.; Bras, W.; Segalman, R. A. Increased Order–Disorder Transition Temperature for a Rod–Coil Block Copolymer in the Presence of a Magnetic Field. *Macromolecules* **2011**, *44*, 7503–7507.
- (45) Kim, J.-S.; Kim, Y.; Kim, H.-J.; Kim, H. J.; Yang, H.; Jung, Y. S.; Stein, G. E.; Kim, B. J. Regioregularity-Driven Morphological Transition of Poly(3-Hexylthiophene)-Based Block Copolymers. *Macromolecules* **2017**, *50*, 1902–1908.
- (46) Yang, C.; Li, Q.; Cai, C.; Lin, J. Nanoparticle-Induced Ellipse-to-Vesicle Morphology Transition of Rod–Coil–Rod Triblock Copolymer Aggregates. *Langmuir* **2016**, *32*, 6917–6927.
- (47) Shi, L.-Y.; Zhou, Y.; Fan, X.-H.; Shen, Z. Remarkably Rich Variety of Nanostructures and Order–Order Transitions in a Rod–Coil Diblock Copolymer. *Macromolecules* **2013**, *46*, 5308–5316.
- (48) Matsen, M. W. Effect of Architecture on the Phase Behavior of AB-Type Block Copolymer Melts. *Macromolecules* **2012**, *45*, 2161–2165.
- (49) Salvatore, S.; Demetriadou, A.; Vignolini, S.; Oh, S. S.; Wuestner, S.; Yufa, N. A.; Stefk, M.; Wiesner, U.; Baumberg, J. J.; Hess, O.; Steiner, U. Tunable 3D Extended Self-Assembled Gold Metamaterials with Enhanced Light Transmission. *Adv. Mater.* **2013**, *25*, 2713–2716.
- (50) Vignolini, S.; Yufa, N. A.; Cunha, P. S.; Guldin, S.; Rushkin, I.; Stefk, M.; Hur, K.; Wiesner, U.; Baumberg, J. J.; Steiner, U. A 3D Optical Metamaterial Made by Self-Assembly. *Adv. Mater.* **2012**, *24*, OP23–OP27.
- (51) Moon, J. H.; Yang, S. Chemical Aspects of Three-Dimensional Photonic Crystals. *Chem. Rev.* **2010**, *110*, 547–574.
- (52) Dolan, J. A.; Wilts, B. D.; Vignolini, S.; Baumberg, J. J.; Steiner, U.; Wilkinson, T. D. Optical Properties of Gyroid Structured Materials: From Photonic Crystals to Metamaterials. *Adv. Adv. Opt. Mater.* **2015**, *3*, 12–32.
- (53) Liu, C.-L.; Lin, C.-H.; Kuo, C.-C.; Lin, S.-T.; Chen, W.-C. Conjugated Rod–Coil Block Copolymers: Synthesis, Morphology, Photophysical Properties, and Stimuli-Responsive Applications. *Prog. Polym. Sci.* **2011**, *36*, 603–637.
- (54) Olsen, B. D.; Segalman, R. A. Self-Assembly of Rod–Coil Block Copolymers. *Mater. Sci. Eng., R* **2008**, *62*, 37–66.
- (55) Lee, M.; Cho, B.-K.; Zin, W.-C. Supramolecular Structures from Rod–Coil Block Copolymers. *Chem. Rev.* **2001**, *101*, 3869–3892.
- (56) Yoon, J.; Lee, W.; Thomas, E. L. Self-Assembly of Block Copolymers for Photonic-Bandgap Materials. *MRS Bull.* **2005**, *30*, 721–726.
- (57) Bockstaller, M.; Kolb, R.; Thomas, E. L. Metallodielectric Photonic Crystals Based on Diblock Copolymers. *Adv. Mater.* **2001**, *13*, 1783–1786.
- (58) Paradiso, S. P.; Delaney, K. T.; Fredrickson, G. H. Swarm Intelligence Platform for Multiblock Polymer Inverse Formulation Design. *ACS Macro Lett.* **2016**, *5*, 972–976.
- (59) Khadilkar, M. R.; Paradiso, S.; Delaney, K. T.; Fredrickson, G. H. Inverse Design of Bulk Morphologies in Multiblock Polymers Using Particle Swarm Optimization. *Macromolecules* **2017**, *50*, 6702–6709.
- (60) Qi, S.; Wang, Z.-G. Kinetics of Phase Transitions in Weakly Segregated Block Copolymers: Pseudostable and Transient States. *Phys. Rev. E: Stat. Phys., Plasmas, Fluids, Relat. Interdiscip. Top.* **1997**, *55*, 1682–1697.
- (61) Qi, S.; Wang, Z.-G. Kinetic Pathways of Order-Disorder and Order-Order Transitions in Weakly Segregated Microstructured Systems. *Phys. Rev. Lett.* **1996**, *76*, 1679.
- (62) Sun, T.; Tang, P.; Qiu, F.; Yang, Y.; Shi, A.-C. Formation of Single Gyroid Nanostructure by Order-Order Phase Transition Path in ABC Triblock Terpolymers. *Macromol. Theory Simul.* **2017**, *26*, 26.
- (63) Yu, J.; Liu, F.; Tang, P.; Qiu, F.; Zhang, H.; Yang, Y. Effect of Geometrical Asymmetry on the Phase Behavior of Rod–Coil Diblock Copolymers. *Polymers* **2016**, *8*, 184.

- (64) Singh, C.; Goulian, M.; Liu, A. J.; Fredrickson, G. H. Phase Behavior of Semiflexible Diblock Copolymers. *Macromolecules* **1994**, *27*, 2974–2986.
- (65) Fredrickson, G. H. *The Equilibrium Theory of Inhomogeneous Polymers*; Oxford University Press, 2013.
- (66) Tang, P.; Qiu, F.; Zhang, H.; Yang, Y. Phase Separation Patterns for Diblock Copolymers on Spherical Surfaces: A Finite Volume Method. *Phys. Rev. E: Statistical, nonlinear, and soft matter physics* **2005**, *72*, 016710.
- (67) Tzeremes, G.; Rasmussen, K. Ø.; Lookman, T.; Saxena, A. Efficient Computation of the Structural Phase Behavior of Block Copolymers. *Phys. Rev. E: Stat. Phys., Plasmas, Fluids, Relat. Interdiscip. Top.* **2002**, *65*, 041806.
- (68) Kriksin, Y. A.; Khalatur, P. G. Parallel Algorithm for 3D SCF Simulation of Copolymers with Flexible and Rigid Blocks. *Macromol. Theory Simul.* **2012**, *21*, 382–399.
- (69) E, W.; Ren, W.; Vanden-Eijnden, E. String Method for the Study of Rare Events. *Phys. Rev. B: Condens. Matter Mater. Phys.* **2002**, *66*, 052301.
- (70) E, W.; Ren, W.; Vanden-Eijnden, E. Energy Landscape and Thermally Activated Switching of Submicron-Sized Ferromagnetic Elements. *J. Appl. Phys.* **2003**, *93*, 2275–2282.
- (71) E, W.; Ren, W.; Vanden-Eijnden, E. Simplified and Improved String Method for Computing the Minimum Energy Paths in Barrier-Crossing Events. *J. Chem. Phys.* **2007**, *126*, 164103.
- (72) Sun, T.; Tang, P.; Qiu, F.; Shi, A.-C. Emergence of Ordered Network Mesophases in Kinetic Pathways of Order-Order Transition for Linear ABC Triblock Terpolymers. *Soft Matter* **2016**, *12*, 9769–9785.
- (73) Kim, M. I.; Wakada, T.; Akasaka, S.; Nishitsuji, S.; Saijo, K.; Hasegawa, H.; Ito, K.; Takenaka, M. Stability of the Fddd Phase in Diblock Copolymer Melts. *Macromolecules* **2008**, *41*, 7667–7670.
- (74) Erukhimovich, I. Y. Weak Segregation Theory and Non-Conventional Morphologies in the Ternary ABC Triblock Copolymers. *Eur. Phys. J. E: Soft Matter Biol. Phys.* **2005**, *18*, 383–406.
- (75) Jiang, K.; Wang, C.; Huang, Y.; Zhang, P. Discovery of New Metastable Patterns in Diblock Copolymers. *Commun. Comput. Phys.* **2013**, *14*, 443–460.
- (76) Majewski, P. W.; Yager, K. G. Reordering Transitions During Annealing of Block Copolymer Cylinder Phases. *Soft Matter* **2016**, *12*, 281–294.
- (77) Yager, K. G.; Forrey, C.; Singh, G.; Satija, S. K.; Page, K. A.; Patton, D. L.; Douglas, J. F.; Jones, R. L.; Karim, A. Thermally-Induced Transition of Lamellae Orientation in Block-Copolymer Films on 'Neutral' Nanoparticle-Coated Substrates. *Soft Matter* **2015**, *11*, 5154–5167.
- (78) Fredrickson, G. H.; Helfand, E. Fluctuation Effects in the Theory of Microphase Separation in Block Copolymers. *J. Chem. Phys.* **1987**, *87*, 697–705.
- (79) Matsen, M. W.; Bates, F. S. Block Copolymer Microstructures in the Intermediate-Segregation Regime. *J. Chem. Phys.* **1997**, *106*, 2436–2448.